Explosive synchronization with asymmetric frequency distribution

Wenchang Zhou,[1,*] Lumin Chen,[1,2,*] Hongjie Bi,[1] Xin Hu,[1] Zonghua Liu,[1,3] and Shuguang Guan[1,3,†]

[1]*Department of Physics, East China Normal University, Shanghai, 200241, China*

[2]*Management School, The University of Sheffield, Western Bank, Sheffield S10 2TN, United Kingdom*

[3]*State Key Laboratory of Theoretical Physics, Institute of Theoretical Physics, Chinese Academy of Sciences, Beijing 100190, China*

(Received 12 February 2015; revised manuscript received 4 June 2015; published 16 July 2015)

In this work, we study the synchronization in a generalized Kuramoto model with frequency-weighted coupling. In particular, we focus on the situations in which the frequency distributions of oscillators are asymmetric. For typical unimodal frequency distributions, such as Lorentzian, Gaussian, triangle, and even special Rayleigh, we find that the synchronization transition in the model generally converts from the first order to the second order as the central frequency shifts toward positive direction. We characterize two interesting coherent states in the system: In the former, two phase-locking clusters are formed, rotating with the same frequency. They correspond to those oscillators with relatively high frequencies while the oscillators with relatively small frequencies are not entrained. In the latter, two phase-locking clusters rotate with different frequencies, leading to the oscillation of the order parameter. We further conduct theoretical analysis to reveal the relation between the asymmetric frequency distribution and the conversion of synchronization type, and justify the coherent states observed in the system.

DOI: 10.1103/PhysRevE.92.012812 PACS number(s): 89.75.Hc, 05.45.Xt, 68.18.Jk

I. INTRODUCTION

The models of coupled oscillators naturally describe various complex systems, in which a large number of individual elements interact with each other [1], such as synchronizing fireflies, neurons in human brain, cardiac pacemaker cells, power grids, and Josephson junction arrays, just to name a few. The Kuramoto model is a prototype in studying synchronization issues [2], in which N phase oscillators are coupled as follows:

$$\dot{\theta}_j = \omega_j + \frac{\kappa}{N}\sum_{n=1}^{N}\sin(\theta_n - \theta_j), \quad j = 1,\ldots,N. \tag{1}$$

Here, θ_j (ω_j) are the instantaneous phase (the natural frequency) of the jth oscillator. Dot denotes the temporal derivative, and κ is the global coupling strength. The set of N natural frequencies $\{\omega_j\}$ is drawn from certain frequency distribution (FD) $g(\omega)$. It has been shown that with the increase of the coupling strength, the system will bifurcate from the incoherent state, in which oscillators rotate almost according to their natural frequencies, into the (partially) coherent state, in which part of oscillators become phase locked to the mean field. As the consequence, an order parameter characterizing the collective behavior in the system transits from 0 to a value that is significantly greater than 0.

For decades, the Kuramoto model has been extensively investigated due to its rich dynamics and simplicity for theoretical treatment [3,4]. In most cases, the relevant synchronization transitions were found to be continuous, i.e., the second order. Recently, Gómez-Gardeñes *et al.* investigated a generalized Kuramoto model on a scale-free network [5]. It is shown that when the natural frequencies of oscillators are correlated with the network topology, i.e., $\omega_j = k_j$, where ω_j and k_j are the natural frequency and degree of the jth oscillator or node in the network, respectively, the order parameter characterizing the coherence in the system experiences a discontinuous jump at certain coupling strength. This so-called explosive synchronization (ES) actually refers to the discontinuous, or the first-order, irreversible synchronization transition, which is drastically different from the second-order transitions observed in the previous studies of the Kuramoto model. Since then, this important finding has stimulated much research attention along this line [6–22].

In particular, Zhang *et al.* found that the correlation between ω_j and k_j in Ref. [5] actually is equivalent to a frequency weight in the coupling strength [12]. Accordingly, a frequency-weighted generalized Kuramoto model was proposed as

$$\dot{\theta}_j = \omega_j + \frac{\kappa|\omega_j|}{N}\sum_{n=1}^{N}\sin(\theta_n - \theta_j), \quad j = 1,\ldots,N. \tag{2}$$

It is shown that ES can generally occur for various network topologies in this model, including the scale-free network. Furthermore, Hu *et al.* obtained the exact solutions of this model, including the transition points and stabilities for both the forward and backward transitions, proving the first-order nature of ES in this model [18]. Based on this model, the mechanism for the first-order synchronization transition has been understood in terms of certain suppressive rules that always limit the formation of large synchronous clusters in such systems [21].

For the classical Kuramoto model, the most important characteristic is its invariance under rotation transformation, i.e., it has rotation symmetry. This can be easily verified by applying the following rotation transformation:

$$\theta_j = \theta_j' + \Omega t, \quad \omega_j = \omega_j' + \Omega, \tag{3}$$

to Eq. (1). Due to this inherent symmetry, the FD $g(\omega)$ can be conveniently chosen to be centered at 0, which is exactly the case in most previous studies of the Kuramoto model. However, for the frequency-weighted model, the

*Authors contributed equally to this work.

†Corresponding author: guanshuguang@hotmail.com

TABLE I. Summary of typical unimodal FDs used in this study.

FD	Formula	Parameter
Lorentzian	$g(\omega)=\frac{\Delta}{\pi[(\omega-\omega_0)^2+\Delta^2]}$	$\Delta=1$
Gaussian	$g(\omega)=\frac{1}{\sqrt{2\pi}\Delta}\exp[\frac{-(\omega-\omega_0)^2}{2\Delta^2}]$	$\Delta=1$
Triangle	$g(\omega)=(\Delta-\lvert\omega-\omega_0\rvert)/\Delta^2, \lvert\omega-\omega_0\rvert<\Delta$	$\Delta=0.1$
Rayleigh	$g(\omega)=\frac{\omega-\omega_0}{\Delta^2}\exp[-\frac{(\omega-\omega_0)^2}{2\Delta^2}]$	$\Delta=1$

dynamical equation (2) is no longer invariant under rotation transformation. This raises an important question: How does the model behave with an asymmetric FD? In this paper, we address this question by numerical simulations and theoretical analysis.

Without losing generality, we consider the typical unimodal FDs, such as Lorentzian, Gaussian, triangle. Moreover, we also consider a special unimodal FD, i.e., the Rayleigh distribution. For convenience of narration, we take the Lorentzian FD as example to report our results. As shown in Table I, there are two parameters in Lorentzian, Gaussian, and triangle FD: ω_0 and Δ. ω_0 corresponds to the central frequency, and Δ controls the width of the FD. Most importantly, we consider the situation $\omega_0 \neq 0$ in the current study. For Rayleigh FD, it is inherently asymmetric, i.e., it cannot become symmetric by translation of axis, which is essentially different from the above three cases. Note that ω_0 in Rayleigh FD does not correspond to the central frequency.

For simplicity, the network is supposed to be globally coupled. Numerical integrations for coupled ordinary differential equations are carried out by the fourth-order Runge-Kutta method with time step 0.01. The initial conditions for the phase variables are random. In both forward and backward transitions, the order parameters are calculated in an adiabatic way, where κ is increased at a step of 0.02 and the final state for a prior κ is used as the initial state for a next κ. For each κ, the order parameters are averaged in a time window after the transient stage. Typically, the total number of oscillators is $N = 10\,000$. Such numerical schemes are adopted throughout this paper.

II. NUMERICAL RESULTS

A. Transitions

We first report the results of numerical simulations to Eq. (2). By default, the results are for Lorentzian FD unless otherwise specified. To characterize the phase synchronization in the model, an order parameter can be defined as

$$re^{i\psi}=\frac{1}{N}\sum_{j=1}^{N}e^{i\theta_j}, \tag{4}$$

where r and ψ are the module and argument of the mean field, respectively. Geometrically, the complex order parameter can be regarded as a vector on the complex plane. According to its definition, r is between 0 and 1. Typically, $r = 0$ indicates a totally random phase distribution, i.e., the incoherent state; while $r > 0$ indicates a (partially) phase-locking state, i.e., the coherent or synchronized state. As the system becomes more coherent, r will gradually approach 1.

We notice that there are two parameters in the asymmetric Lorentzian FD, i.e., the central frequency ω_0 and the width at half maximum Δ (see the formula in Table I). To simplify the situation, we keep Δ as a constant, i.e., $\Delta = 1$ in this work. We change ω_0 to shift the FD along positive axis and investigate the synchronization transition in Eq. (2), i.e., how r changes with respect to the coupling strength κ.

Figure 1 plots the phase diagrams for the system with different central frequencies ω_0. Generally, we observe both first- and second-order synchronization transitions in the system. When $\omega_0 = 0$, i.e., for the symmetric FD, it has been proven that the synchronization transition is discontinuous [18]. When ω_0 is small, it is found that this discontinuous transition remains. A typical example is given in Fig. 1(a), where $\omega_0 = 0.3$. When ω_0 is further increased, it is found that the hysteresis area significantly shrinks if we compare Fig. 1(b) ($\omega_0 = 0.5$) with Fig. 1(a) ($\omega_0 = 0.3$). A careful examination reveals that the shrinking of the hysteresis area is due to the decrease of the forward transition point κ_f, while the backward transition point κ_b almost remains unchanged within the precision of our numerical simulations. As ω_0 increases, the forward transition point κ_f becomes smaller and smaller. Numerically, we find that when $\omega_0 \geqslant 0.7$, there are two transitions in the forward process. Now, the first transition is continuous, i.e., the second order, and the second transition is explosive, i.e., the first order. A typical example has been shown in Fig. 1(c), where it is seen that a small hysteresis area still remains. As ω_0 further increases, the hysteresis area finally vanishes. After that, the system will undergo a continuous synchronization transition, similar to the classical Kuramoto model. A typical example is illustrated in Fig. 1(d), where $\omega_0 = 1.2$.

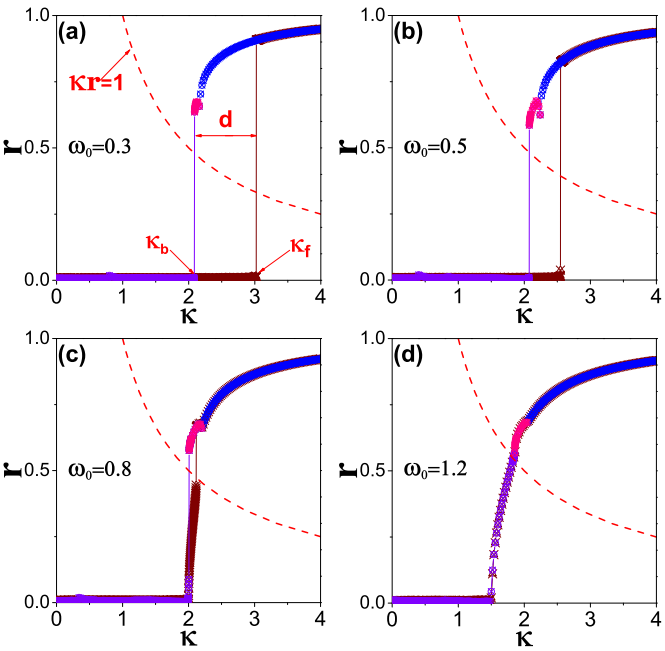

FIG. 1. (Color online) The order parameter r vs the coupling strength κ. It is shown that with the increase of ω_0, the synchronization transition converts from the first-order type into the second-order one. From (a) to (d), $\omega_0 = 0.3, 0.5, 0.8, 1.2$, respectively. The dashed lines correspond to $\kappa r = 1$. Lorentzian FD is used for Figs. 1 to 6. $\Delta = 1$ and $N = 10\,000$ are the same throughout this paper.

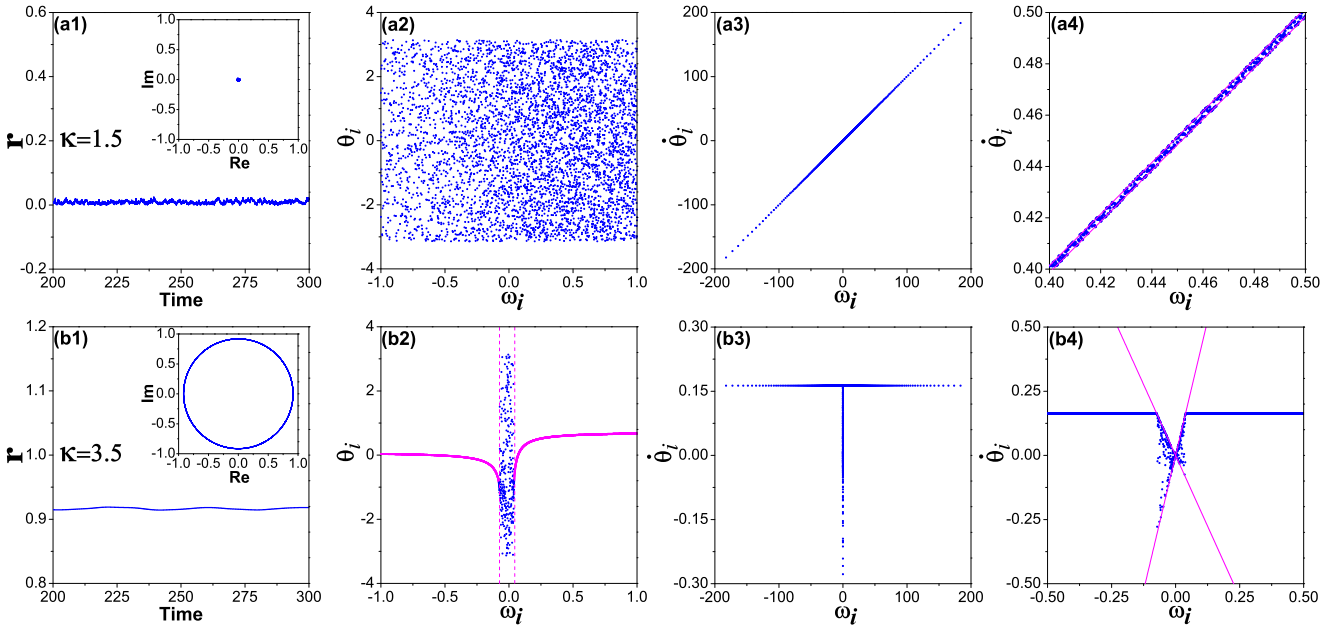

FIG. 2. (Color online) Characterization of the steady states in the forward continuity of the first-order transition. $\omega_0 = 0.5$. Rows (a) and (b) correspond to $\kappa = 1.5$ and 3.5, respectively. Columns 1–3 correspond to the order parameter, the distributions of the instantaneous phases and frequencies, respectively. Column 4 is the enlargement of column 3. Throughout this paper, the purple dashed line, such as that in (b2), denotes the boundary of synchronized clusters predicted by Eq. (9), and the purple straight lines, such as those in (a4) and (b4), denote the fluctuation range of instantaneous frequencies of oscillators predicted by Eq. (11).

B. Steady states in the first-order transition

Through extensive simulations, we find that the model can exhibit rich steady states. To characterize them, we study both the macroscopic property, i.e., the order parameter, and the microscopic properties, such as the distributions of phases and instantaneous frequencies. The results are shown in Figs. 2–5. In the following, we describe them in detail.

We first report the steady states in the first-order synchronization transition. In this case, the system undergoes different paths in the phase diagram when the coupling strength increases or decreases. We take $\omega_0 = 0.5$ as an example. The corresponding phase diagram has been shown in Fig. 1(b). For the forward transition process, there are two steady states: one is the trivial incoherent state, and the other is a (partially) coherent state. In Figs. 2(a1) and 2(b1), the order parameters of these two steady states are plotted, corresponding to $\kappa = 1.5$ and 3.5, respectively. It is seen that in the former case, the order parameter is almost 0, while in the latter case, it is greater than 0.9, indicating the occurrence of high coherence in the system when the coupling strength is large enough. In this coherent state, it is seen that there are two phase-locking clusters and some drifting oscillators. Interestingly, the oscillators with relatively large natural frequencies are phase locked, while the oscillators with relatively small natural frequencies are drifting, as shown in Fig. 2(b2). This scenario is different from the coherent state in classical Kuramoto model, where the oscillators with relatively small natural frequencies are typically easier to be entrained by the mean field. Although the oscillators are divided into two clusters with different phases, they have almost the same instantaneous frequencies, as shown in Figs. 2(b3) and 2(b4). So, their relative positions are unchanged during rotation on the complex plane.

For the backward transition process, there are three typical steady states as the coupling strength goes down. The first one is the coherent state, i.e., the partially synchronized state, which is essentially the same as in the forward transition process when κ is large. An example has been shown in Fig. 3(a1). Interestingly, when κ decreases below the knee point [see Fig. 1(b)] into the hysteresis area, another type of coherent state appears. We show one such example in Fig. 3(b1). As shown in the figure, in this state, the order parameter oscillates almost "periodically." However, when we plot the order parameter in the complex plane, we find that the mean-field vector does not form a closed orbit. Instead, it is seemingly ergodic, which reminds us of certain quasiperiodical motion. when the coupling strength κ further decreases, a first-order backward transition occurs. After that, the order parameter drops to almost 0, coinciding with the order parameter in the forward transition. Macroscopically, the system exhibits no collective behavior in both forward and backward transition processes at this stage. However, the incoherent state in the backward transition is nontrivial. One such example is shown in Fig. 3(c1), where $\kappa = 1.5$ and $r \approx 0$. Comparing this figure with Fig. 2(a1), we find that, microscopically, there are essential differences between these two incoherent states. As shown in Fig. 3(c2), although the phase seems to be randomly distributed, there are many small clusters with fine structures. Similar fine structures can also be seen in the distribution of the instantaneous frequencies although they are basically distributed around their natural frequencies [Figs. 3(c3) and 3(c4)].

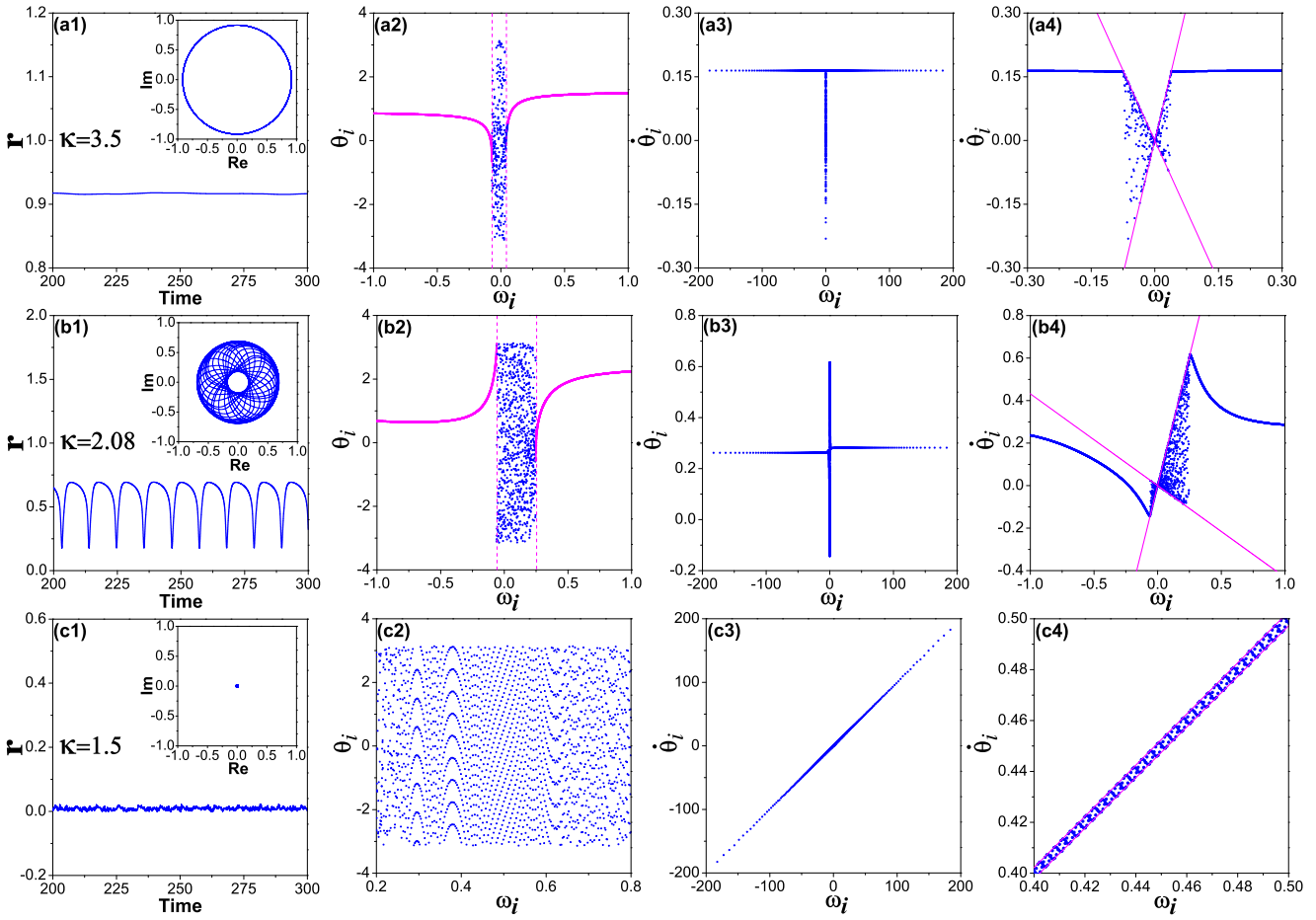

FIG. 3. (Color online) Characterization of the steady states in the backward continuity of the first-order transition. $\omega_0 = 0.5$. Rows (a)–(c) correspond to $\kappa = 3.5$, 2.08, and 1.5, respectively. The parameters and the arrangement of panels are the same as in Fig. 2.

C. Steady states in the second-order transition

We then characterize the coherent states in the second-order transition process. In this case, the order parameter follows the same path in the phase diagram when the coupling strength increases or decreases. We take $\omega_0 = 1.2$ as an example. The corresponding phase diagram has been shown in Fig. 1(d).

In Fig. 4, we show the typical steady states observed in the forward continuity, including the incoherent state [Fig. 4(a1)], the coherent state [Figs. 4(b1) and 4(d1)], and the oscillating coherent state [Fig. 4(c1)]. It is found that there exist two types of (partially) coherent states. Figures 4(b1) and 4(d1) are two typical examples. We classify them as types I and II, respectively. For the type-I coherent state, it is seen that there is only one phase-locking cluster, corresponding to oscillators with relatively small natural frequencies. However, for the type-II coherent state, there are two phase-locking clusters which correspond to oscillators with relatively high natural frequencies. In this state, the oscillators with relatively small natural frequencies are not entrained. They are still drifting. In fact, the coherent states in the first-order transition, as shown in Figs. 2(b1) and 3(a1), also belong to this type.

For the backward continuity, the order parameter follows the same path as that in the forward one [Fig. 1(d)]. However, we have specially checked the steady states for comparison. The results are shown in Fig. 5. Comparing with Fig. 4, it is found that the oscillating coherent state and the coherent states (I and II) are qualitatively the same in both forward and backward continuity. Similar to the situation of the first-order transition, the incoherent state in the backward transition is nontrivial although the transition is the second order in this parameter regime.

D. Typical unimodal FDs

In the above, we report the results for the Lorentzian FD. In fact, as listed in Table I, we have considered several typical unimodal FDs in this study, including the special Rayleigh FD. By extensive numerical simulations, we have investigated the phase diagrams of synchronization and characterized the typical coherent states in the system. The results are shown in Fig. 6. Similarly, we observe the conversion from first-order to second-order transition, and type-I and type-II coherent states. These results show that the model (2) exhibits universal behaviors under asymmetric FDs, which certainly deserves further theoretical analysis as we will do in the following section.

III. THEORETICAL ANALYSIS

A. Coherent states

By carefully examining the steady states observed above, we find that in the type-I coherent states, such as Figs. 4(b)

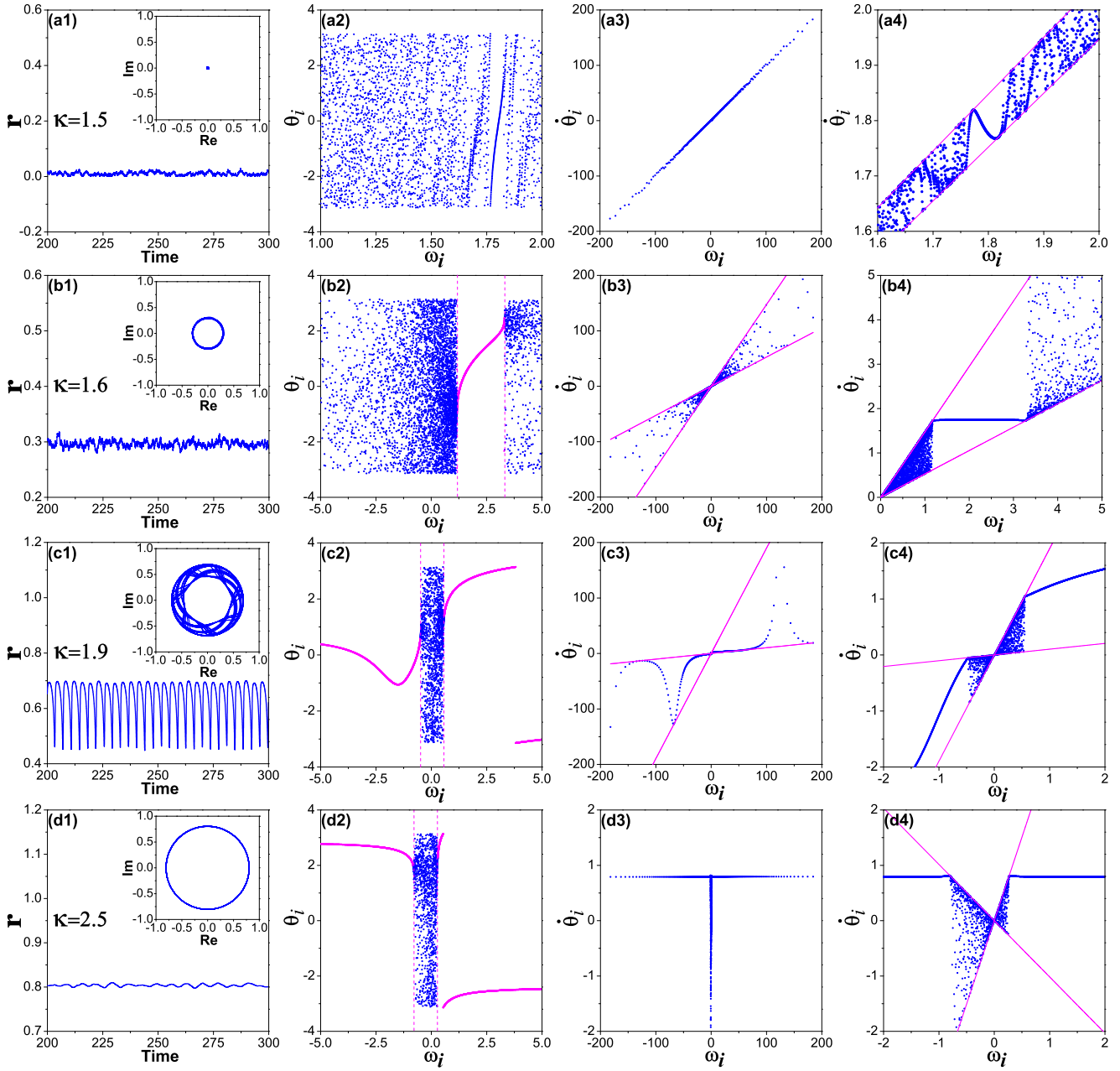

FIG. 4. (Color online) Characterization of the steady states in the forward continuity of the second-order transition. $\omega_0 = 1.2$. Rows (a)–(d) correspond to $\kappa = 1.5$, 1.6, 1.9, and 2.5, respectively. The parameters and the arrangement of panels are the same as in Fig. 2.

and 5(c), the oscillators with relatively small frequencies are phase locked, while the oscillators with relatively large frequencies are drifting. This is consistent with the physical picture in the classical Kuramoto model. However, in the type-II coherent states, such as Figs. 2(b), 3(a), 4(d), and 5(a), and in the oscillating coherent states, such as Figs. 3(b), 4(c), and 5(b), on the contrary, the oscillators with relatively large frequencies are phase locked, while the oscillators with relatively small frequencies are drifting. This situation is seemingly opposite to our understanding of synchronization of phase oscillators. How could this happen? In the following, we conduct a mean-field analysis to answer this question.

In the mean-field form, Eq. (2) becomes

$$\dot{\theta}_j = \omega_j + \kappa r|\omega_j| \sin(\psi - \theta_j), \quad j = 1, \ldots, N. \qquad (5)$$

The most important characteristic of this equation is that the effective coupling $\kappa|\omega_i|$ is proportional to the magnitude of the natural frequency. For symmetric FDs, the average instantaneous frequency for all oscillators is always 0. Therefore, in the coherent state, the average phase ψ is a constant. We then can use the above mean-field equation to determine the phase-locking condition. As analyzed in Ref. [18], for typical symmetric FDs, all oscillators in this system will explosively jump to the coherent state when the coupling strength is large enough. The system has no partially coherent state with symmetric FDs. In its coherent state, two clusters are formed, corresponding to the populations of positive and negative frequencies, respectively. Inside each cluster, all oscillators totally coincide with each other, just like one oscillator, which

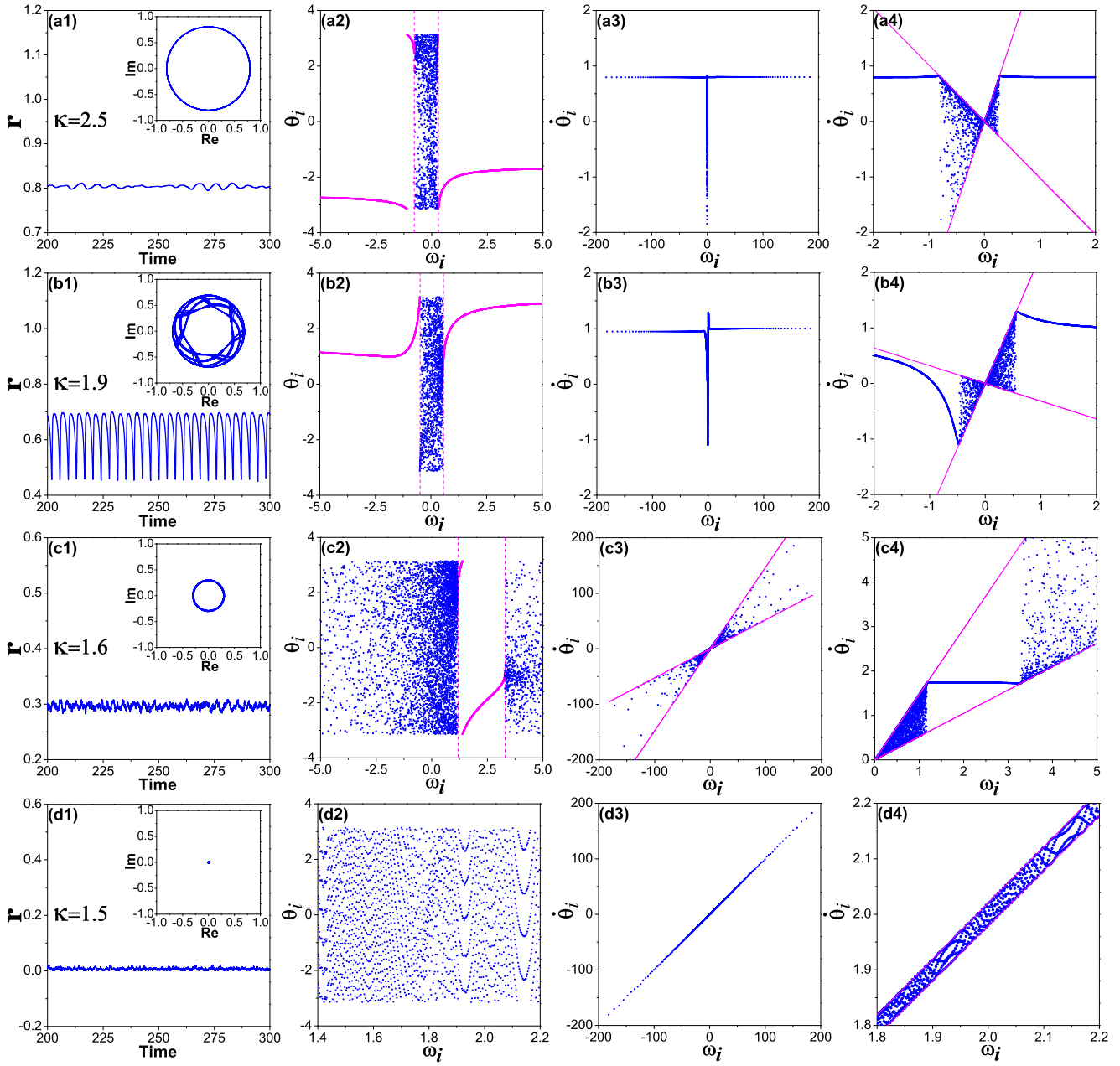

FIG. 5. (Color online) Characterization of the steady states in the backward continuity of the second-order transition. $\omega_0 = 1.2$. Rows (a)–(d) correspond to $\kappa = 2.5$, 1.9, 1.6, and 1.5, respectively. The parameters and the arrangement of panels are the same as in Fig. 2.

keeps fixed in phase space. So, this is actually a trivial coherent state.

Compared with the trivial coherent state in Eq. (2) with symmetric FDs, the nontrivial coherent states in Eq. (2) with asymmetric FDs are interesting. Apparently, they should originate from the asymmetry of FDs used. However, for asymmetric FDs, the average instantaneous frequency for all oscillators is not 0. In this case, we will generally observe traveling wave states in which the synchronized clusters of oscillators rotate [e.g., see Figs. 4(b4), (c4), and (d4)] and the average phase ψ is time dependent. Therefore, Eq. (5) generally has no solution of fixed point, and it cannot be directly used to obtain the phase-locking condition as done for the situations of symmetric FDs. To deal with this situation, we apply the rotation transformation

$$\theta_j = \theta'_j + \omega_0 t,\ \omega_j = \omega'_j + \omega_0 \tag{6}$$

to Eq. (2). This gives the following equation:

$$\dot{\theta}'_j = \omega'_j + \frac{\kappa|\omega'_j + \omega_0|}{N}\sum_{n=1}^{N}\sin(\theta'_n - \theta'_j), \quad j = 1,\ldots,N. \tag{7}$$

The above rotation transformation is equivalent to observing the motion of oscillators in a rotating frame with frequency ω_0. In the rotating frame, the distribution of frequency ω' is symmetric to 0 now, and the average instantaneous frequencies equal to 0 accordingly. Therefore, we can use the

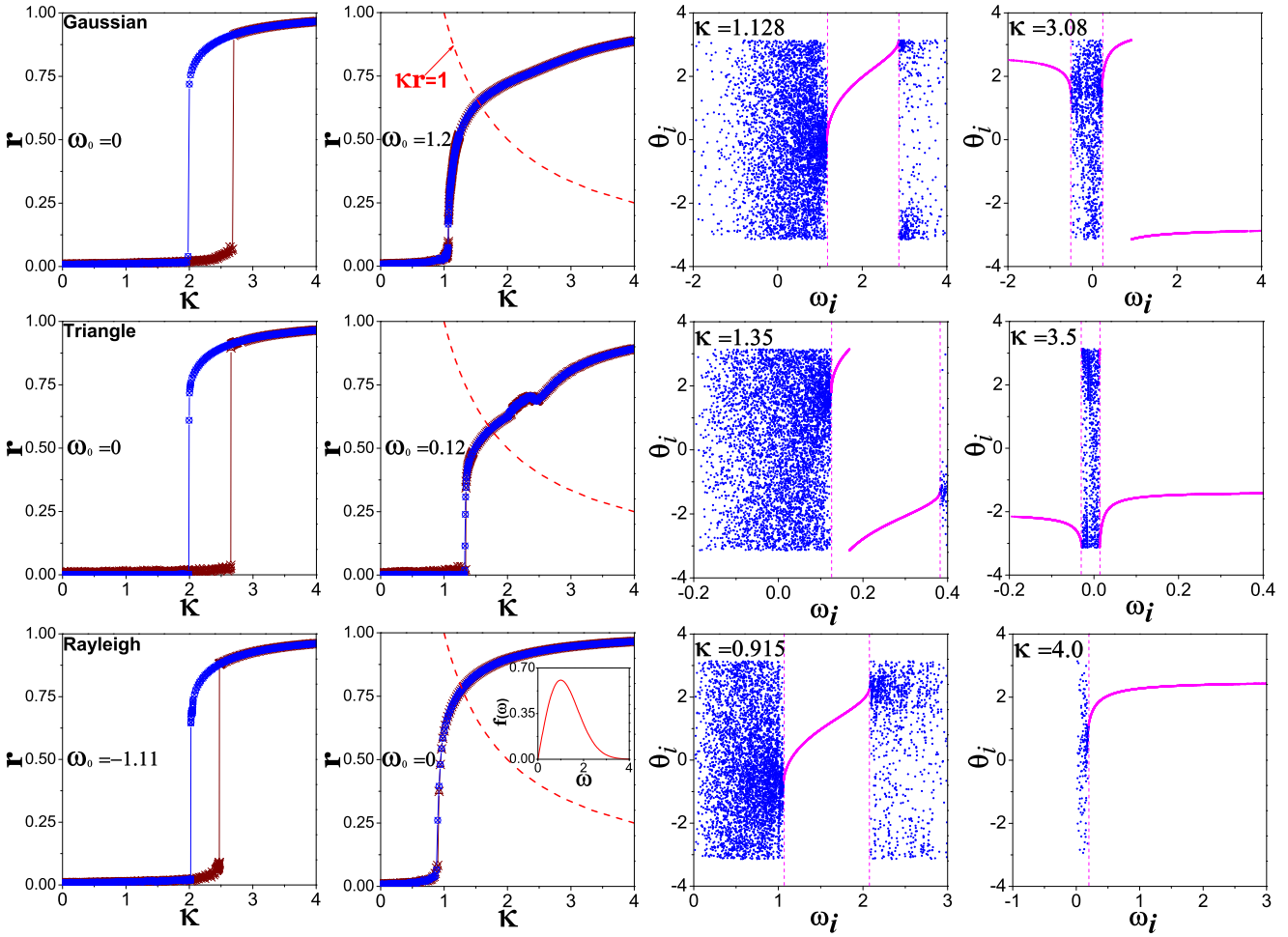

FIG. 6. (Color online) Characterization of synchronization and the steady states in model (2) with other typical FDs. Rows (a)–(c) correspond to Gaussian, triangle, and Rayleigh FD, respectively. It is shown that the system generally converts from first-order transition to second-order one as the FD shifts towards positive direction. Columns 3 and 4 characterize the type-I and type-II coherent states corresponding to column 2, respectively. The inset plots the Rayleigh FD that is inherently asymmetric.

corresponding mean-field equation

$$\dot{\theta}'_j = \omega'_j + \kappa r|\omega'_j + \omega_0|\sin(\psi - \theta'_j), \quad j = 1, \ldots, N \tag{8}$$

to determine the phase-locking condition. Equation (8) indicates that each oscillator is entrained by the mean field r with the effective coupling strength $\kappa|\omega'_j + \omega_0|$. When $\omega_0 = 0$, i.e., the FD is symmetric, the entraining force is exactly proportional to the natural frequency of the oscillator, leading to ES in the system [18]. When $\omega_0 \neq 0$, i.e., for the asymmetric FDs, there is a mismatch between the natural frequency and the entraining force of the oscillator. This will essentially change the synchronization behaviors of oscillators in the system. From Eq. (8), we obtain the phase-locking condition for oscillators as

$$f(\omega') = \left|\frac{\omega'_j}{\omega'_j + \omega_0}\right| \leqslant \kappa r, \quad j = 1, \ldots, N. \tag{9}$$

In Fig. 7, we plot the function $f(\omega')$. Based on the above results of numerical simulations and theoretical analysis, now we can understand the physical picture of the collective dynamics observed in the model.

(1) *Type-I coherent state*. From Fig. 7, when $\kappa r \leqslant 1$, there will be one phase-locking cluster which consists of oscillators with relatively small natural frequencies, rotating with certain frequency. In the meantime, the oscillators with relatively large natural frequencies are drifting. Such examples have been shown in Figs. 4(b) and 5(c). In the phase diagram of Fig. 1, we have verified that these states locate below the curve $\kappa r = 1$.

(2) *Type-II coherent state*. From Fig. 7, when $\kappa r > 1$, due to the singularity located at the $\omega\prime = -\omega_0$, there will be two phase-locking clusters, consisting of oscillators with relatively large natural frequencies. Depending on the magnitude of the coupling strength κ, there will be two situations. When κ is large enough, the two phase-locking clusters almost lock into one frequency. In fact, they can be understood as one cluster with two separated phases. The key point here is that all oscillators in the coherent clusters rotate with almost the same frequency. As a result, the order parameters almost keep constant in these cases. Such examples have been shown in Figs. 2(b), 3(a), 4(d), and 5(a). In the phase diagram of Fig. 1,

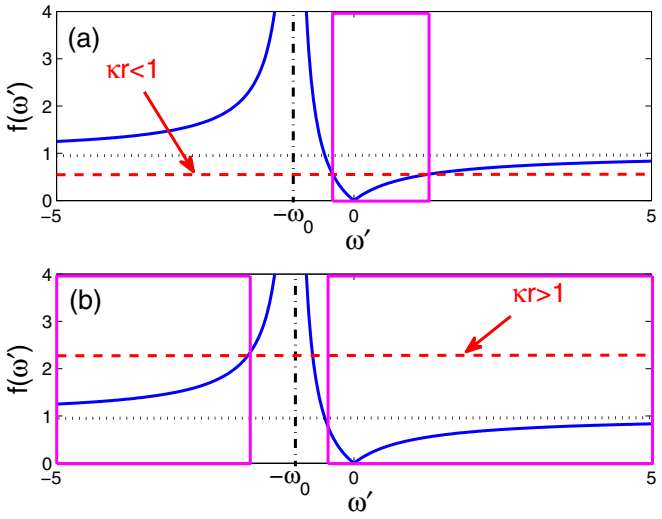

FIG. 7. (Color online) Illustration of the phase-locking condition for Eq. (2). The blue curve is $f(\omega')$ that is defined in Eq. (9). The red dashed line is κr, which intersects with $f(\omega')$ and determines the phase-locking region for frequency ω', as shown by the purple rectangle. (a) Corresponds to the situation of type-I coherent states. (b) Corresponds to the situation of type-II and oscillating coherent states. In Figs. 1 to 6, we have marked the theoretical synchronization areas by purple dashed lines. The theoretical results are well consistent with the numerical ones.

we have verified that these states all locate above the curve $\kappa r > 1$.

(3) *Oscillating coherent state*. When $\kappa r > 1$, but κ is not large enough to keep the phase-locking oscillators locked to one frequency, the oscillators split into two clusters with different rotating frequencies. As we know, if two oscillators rotate with two different constant frequencies along the unit circle, the resultant order parameter will oscillate. However, since the distribution of instantaneous frequencies changes with time, the average frequencies of the two rotating clusters also vary with time. As a consequence, we observe approximately periodical oscillation of order parameter. In Fig. 8, we also show the results of power spectrum analysis to the time series $x(t)$, which apparently exhibits behavior similar

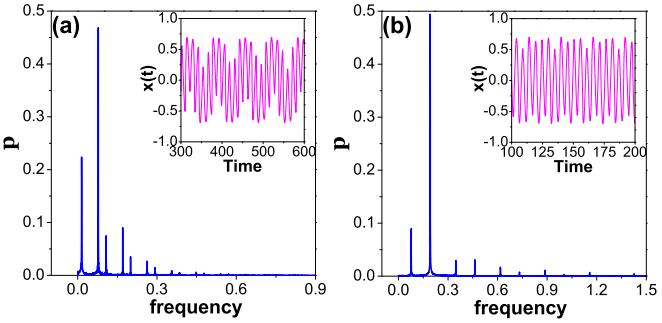

FIG. 8. (Color online) Characterization of the quasiperiodical property for the time series $x(t) = \mathrm{Re}[r(t)]$ in oscillating coherent states. (a), (b) Correspond to the situations in Figs. 3(b1) and 4(c1), respectively. The first two "spectrum lines" correspond to the dominant frequencies of the time series.

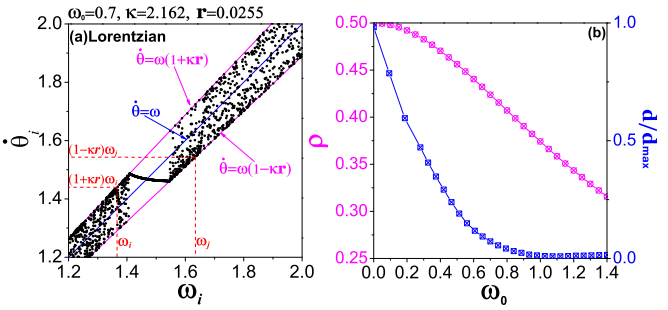

FIG. 9. (Color online) (a) A schematic illustration for the phase-locking condition between two oscillators, i.e., Eqs. (12) and (13). (b) Characterization the conversion from the first-order transition to the second-order one by ρ vs ω_0 (the circles) and $d/d_{\max}$ vs ω_0 (the squares). d denotes the width of hysteresis loop, as shown in Fig. 1(a). $d_{\max} = 2$ is the largest width of hysteresis loop when $\omega_0 = 0$. Note that different scalings are used for ρ (the left axis) and $d/d_{\max}$ (the right axis) for better visualization. Other parameters are the same as in Fig. 1.

to "beat" phenomenon. It is verified that these time series always comprise two dominant frequencies. Usually, they are irreducible, leading to the quasiperiodicity of the order parameter on complex plane.

In addition, the system also exhibits trivial and nontrivial incoherent states [see Figs. 3(c) and 5(d)]. In fact, in the backward continuity the system actually undergoes desynchronization process. The small local fine clusters in the nontrivial coherent state just reflect the "memory" of the initial coherent state.

B. Conversion from explosive to continuous transition

As shown in Figs. 1 and 6, the model exhibits another interesting characteristic: the type of synchronization converts from the first order to the second order as the FD is translated toward the positive direction in axis. Why does ω_0 regulate the nature of synchronization transition? This is an important issue. Answering it will not only enhance our understandings to ES, but also shed light on controlling it. In the following, we provide a heuristic argument to address this question.

The mean-field equation (5) can be rewritten as

$$\dot{\theta}_j = \omega_j \pm \kappa r \omega_j \sin(\psi - \theta_j), \quad j = 1, \ldots, N. \tag{10}$$

Its left-hand side is the instantaneous frequency of oscillators. It has two sources as in the right-hand side of the equation. The first term is the natural frequency, and the second term can be understood as the fluctuation around the former. Since the upper bound of sine function is 1, the fluctuation range is between $\pm\kappa r\omega_j$. Therefore, given the coupling strength, the instantaneous frequencies of all coupled oscillators are located between two straight lines as

$$\dot{\theta} = (1 \pm \kappa r)\omega. \tag{11}$$

In Fig. 9(a), we show an example where $\dot{\theta}_i$ is plotted versus ω_i. The two purple straight lines correspond to the above equations. It is seen that all the instantaneous frequencies are distributed following the theoretical prediction. For two arbitrary oscillators i and j, the necessary condition for them

to be phase locked is that their instantaneous frequencies are close enough (or, loosely, equal to each other for simplicity). Therefore, as shown in Fig. 9(a), the phase-locking condition for oscillators i and j is that their ranges of instantaneous frequencies must overlap, i.e., the upper bound of $\dot{\theta}_i$ must be greater than the lower bound of $\dot{\theta}_j$. This leads to the following inequality:

$$(1 + \kappa r)\omega_i > (1 - \kappa r)\omega_j, \tag{12}$$

which gives the phase-locking condition as

$$\Delta\omega_{ij} = \frac{|\omega_j - \omega_i|}{|\omega_j| + |\omega_i|} < \kappa r. \tag{13}$$

Given κ, a pair of oscillators are forbidden to synchronize with each other when the above condition is not satisfied. Therefore, condition (13) is called as the suppressive rule for forming synchronized clusters [21]. For a system of coupled phase oscillators, if condition (13) is easily satisfied for most pairs of oscillators, the small synchronized clusters will gradually grow up and merge with each other to form larger ones as the coupling strength increases, leading to the second-order transition. On the contrary, if a considerable proportion of oscillator pairs violate condition (13), the formation of large clusters in the system is significantly suppressed. In this case, the system has no choice by exhibiting ES when the coupling strength exceeds a certain threshold.

We now analyze which pair of oscillators are mostly possible to violate condition (13). We notice that if a pair of oscillators whose natural frequencies have different sign, $\Delta\omega_{ij} = 1$. How about the magnitude of κr? We can give a reasonable estimate. When κ is small, the system is in the incoherent state, where the order parameter r fluctuates around zero with the amplitude of the order $1/\sqrt{N}$. In our simulation, $N = 10\,000$, so $1/\sqrt{N} = 0.01$. Typically, the order of κ in the incoherent state is less than 10. Thus, we safely estimate the upper bound of κr as 0.1. From the above analysis, it is found that the oscillator pairs with $\Delta\omega_{ij} = 1$ certainly violate condition (13). Since in the asymmetric FDs, the location of the central frequency ω_0 actually controls the ratio between oscillators with positive and negative frequencies, we can define a ratio as

$$\rho(\omega_0) = N(\Delta\omega_{ij} = 1)/N_{\text{all}}, \tag{14}$$

where $N(\Delta\omega_{ij} = 1)$ and N_{all} denote the number of oscillator pairs with $\Delta\omega_{ij} = 1$ and the number of total oscillator pairs, respectively. This quantity characterizes the possibility of occurrence of ES in the system. The larger the ρ, the higher possibility for the first-order synchronization to occur. In Fig. 9(b), we plot ρ versus ω_0. It is seen that when $\omega_0 = 0$, i.e., the symmetric FDs, $\rho = 0.5$. This means that half oscillator pairs in the systems violate condition (13). Typically, the first-order synchronization occurs in this case. As ω_0 increases, ρ continuously decreases, which is in favor of the occurrence of the second-order synchronization transition. This can be verified by the decrease of the width of the hysteresis area d, which is also plotted in Fig. 9(b) for comparison. Numerically, we find that when ρ decreases to a certain value, the synchronization type converts from the first order to the second order, i.e., from explosive to continuous. The above analysis provides a qualitative explanation as to why an explosive transition changes to a continuous one in Eq. (2) when the bias of asymmetric FDs increases.

IV. CONCLUSION

In this work, we investigated the synchronization transition in a frequency-weighted Kuramoto model with typical asymmetric FDs. It is shown that when the bias of central frequency is small, the type of synchronization transition is the first order, i.e., explosive. When it is large, the type of synchronization transition is the second order, i.e., continuous. We characterized the coherent states in both forward and backward continuities, and found that they can be classified into several types, including the type-I and type-II coherent states, and the oscillating coherent state. Under the asymmetric FDs, the coherent states in this model exhibit two new characteristics. One is that the phase-locking oscillators may split into two clusters, but locked to the same frequency. The other is that when the coupling strength is not large enough, the phase-locking oscillators may further split into two clusters with different frequencies, leading to a weaker synchronous state in the system characterized by the oscillation of order parameter. Based on theoretical analysis, we revealed that the above coherent states originate from the mismatch between the natural frequency and the effective coupling strength in the rotating frame due to the asymmetry of FDs. We also provided an analysis to explain the conversion of type of transition in the model. Since most previous works focused on the cases of symmetric FDs, this work is helpful to augment our understandings of the synchronous behaviors in the generalized Kuramoto model.

ACKNOWLEDGMENT

This work is supported by the the Innovation Program of Shanghai Municipal Education Commission Grant No. 12ZZ043; the National Natural Science Foundation of China under Grants No. 11075056, No. 11375066, No. 11305062, and No. 11135001; and the Open Project Program of State Key Laboratory of Theoretical Physics, Institute of Theoretical Physics, Chinese Academy of Sciences, China (Grant No. Y4KF151CJ1).

[1] A. Pikvosky, M. Rosenblum, and J. Kurths, *Synchronization: A Universal Concept in Nonlinear Sciences* (Cambridge University Press, Cambridge, 2003).

[2] Y. Kuramoto, *Chemical Oscillations, Waves, and Turbulence* (Springer, New York, 1984), pp. 75–76.

[3] S. H. Strogatz, Phys. D (Amsterdam) **143**, 1 (2000).

[4] J. A. Acebrón, L. L. Bonilla, C. J. Pérez Vicente, F. Ritort, and R. Spigler, Rev. Mod. Phys. **77**, 137 (2005).
[5] J. Gómez-Gardeñes, S. Gómez, A. Arenas, and Y. Moreno, Phys. Rev. Lett. **106**, 128701 (2011).
[6] I. Leyva, R. Sevilla-Escoboza, J. M. Buldú, I. Sendiña-Nadal, J. Gómez-Gardeñes, A. Arenas, Y. Moreno, S. Gómez, R. Jaimes-Reátegui, and S. Boccaletti, Phys. Rev. Lett. **108**, 168702 (2012).
[7] T. K. D. M. Peron and F. A. Rodrigues, Phys. Rev. E **86**, 056108 (2012); **86**, 016102 (2012).
[8] B. C. Coutinho, A. V. Goltsev, S. N. Dorogovtsev, and J. F. F. Mendes, Phys. Rev. E **87**, 032106 (2013).
[9] P. Ji, T. K. D. M. Peron, P. J. Menck, F. A. Rodrigues, and J. Kurths, Phys. Rev. Lett. **110**, 218701 (2013).
[10] I. Leyva *et al.*, Sci. Rep. **3**, 1281 (2013).
[11] P. Li, K. Zhang, X. Xu, J. Zhang, and M. Small, Phys. Rev. E **87**, 042803 (2013).
[12] X. Zhang, X. Hu, J. Kurths, and Z. Liu, Phys. Rev. E **88**, 010802(R) (2013).
[13] L. Zhu, L. Tian, and D. Shi, Phys. Rev. E **88**, 042921 (2013).
[14] I. Leyva, I. Sendiña-Nadal, J. A. Almendral, A. Navas, S. Olmi, and S. Boccaletti, Phys. Rev. E **88**, 042808 (2013).
[15] W. Liu, Y. Wu, J. Xiao, and M. Zhan, Europhys. Lett. **101**, 38002 (2013).
[16] H. Chen, G. He, F. Huang, C. Shen, and Z. Hou, Chaos **23**, 033124 (2013).
[17] Y. Zou, T. Pereira, M. Small, Z. Liu, and J. Kurths, Phys. Rev. Lett. **112**, 114102 (2014).
[18] X. Hu *et al.*, Sci. Rep. **4**, 7262 (2014).
[19] P. S. Skardal and A. Arenas, Phys. Rev. E **89**, 062811 (2014).
[20] H. Bi *et al.*, Europhys. Lett. **108**, 50003 (2014).
[21] X. Zhang, Y. Zou, S. Boccaletti, and Z. Liu, Sci. Rep. **4**, 5200 (2014).
[22] X. Zhang, S. Boccaletti, S. Guan, and Z. Liu, Phys. Rev. Lett. **114**, 038701 (2015).